A comprehensive comparison of Virtual Synchronous Generators with focus on virtual inertia and frequency regulation

A Comprehensive Comparison of Virtual Synchronous Generators with Focus on Virtual Inertia and Frequency Regulation

Vincenzo Mallemaci*, Fabio Mandrile, Sandro Rubino, Andrea Mazza, Enrico Carpaneto, Radu Bojoi

Dipartimento Energia "G. Ferraris", Politecnico di Torino, Corso Duca degli Abruzzi 24, 10129, Torino, Italy

Abstract

The concept of Virtual Synchronous Generator (VSG) may be used to make grid-connected power electronic converters behave as synchronous generators. VSGs can provide the ancillary services requested by the latest grid codes in a straightforward way, compatible with the already existing structure of power systems and with the advantage of being a digital model with tunable parameters (e.g., inertia constant). This represents a promising solution to mitigate the future reduction of the total power system inertia and the grid stability issues related to both the decommissioning of synchronous generation and the widespread penetration of electronically interfaced renewable power generators (especially solar and wind). Since the literature is rich of VSG models, it is important to have a clear overview of them. Therefore, this paper aims at performing a review and comparison of the active power control and inertial capabilities of ten VSG solutions available in the literature. First, each model is briefly described and a common tuning procedure is proposed to obtain a fair performance comparison. Then, experimental tests are presented to show the behavior of the VSGs.

*Corresponding author
Email address: vincenzo.mallemaci@polito.it (Vincenzo Mallemaci)

Keywords: Virtual Synchronous Generator (VSG), Renewable Energy Source (RES), grid–connected inverter, experimental comparison, virtual inertia, frequency regulation

1. Introduction

In the last decade, the amount of energy generated from Renewable Energy Sources (RESs) increased exponentially and it is expected to rise more and more in the next 20 years [1]. The most promising RES plants are based on solar and wind energy. To interface them with the grid, power electronic converters are needed [2], as shown in the general diagram of Figure 1.1a.

The electric grid guarantees the balance between the demand and the supply of the electric power at every instant, by keeping the grid frequency as close as possible to its nominal value [3]. To do this, the electric grid relies on the alternators of the hydroelectric and thermoelectric power plants. During load transients, they perform a frequency regulation process historically divided into three phases, as shown in Figure 1.1b.

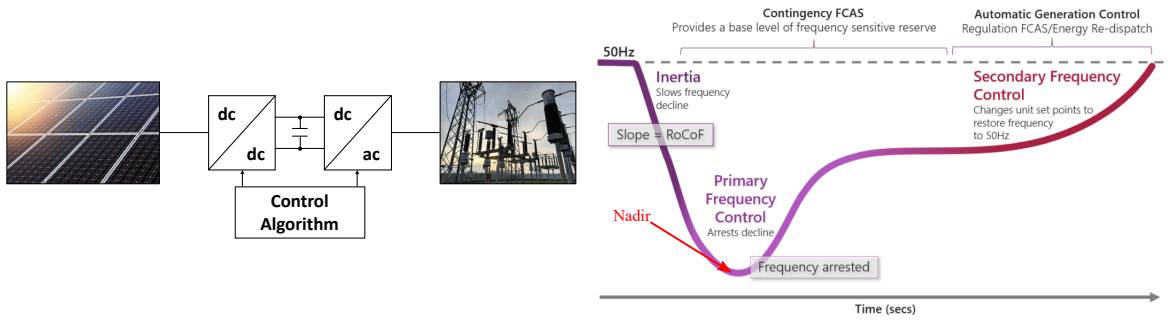

(a) (b)

Figure 1.1: From left to right: (a) Conventional scheme of connection between PV plant and the grid; (b) Frequency profile and frequency control steps after a generation reduction. Source: [4].

When a power imbalance occurs, it is instantly covered by means of the kinetic energy of the alternators: if the power demand increases, the rotors will slow down and inject inertial active power into the grid (inertial behavior). This way, synchronous

generators (SGs) can increase the nadir (minimum frequency value) and reduce the Rate of Change of Frequency (RoCoF), i.e., the frequency derivative, minimizing the likelihood of frequency protection relays to intervene. After these first few seconds (1–4 s), the primary frequency regulation intervenes and modifies the power flow from the sources (e.g., water flow), according to the new load conditions. This operation typically requires some minutes. Finally, the secondary frequency control restores the frequency setpoint of a grid portion (e.g., a country). The secondary frequency control is centralised and actuated in the time scale of tens of minutes.

The inertial behavior and the frequency control are part of the so called ancillary services that rotating power plants have to provide to the electric grid, in order to contribute to its stability [5].

Renewable power generators (RPGs) do not embed inertial features, since power converters are static, without rotating mechanical parts. Moreover, until recent years, RPGs only injected power according to their conventional control algorithm, i.e., Maximum Power Point Tracking (MPPT), and the ancillary services were provided by SGs. However, the future decommissioning of thermoelectric power plants (especially coal-based) will reduce the number of SGs connected to the grid. This implies the decrease of the total power system inertia with two main consequences: higher RoCoF in case of a power imbalance; reduction of the grid frequency constancy. The lower is the inertia, the lower is the grid frequency stability. Therefore, a large penetration of electronically interfaced RPGs could affect the grid correct operation if they do not provide ancillary services (in particular, inertial behavior) as well.

A recent exemplary case is the 2016 South Australia (SA) blackout [6]: tornadoes damaged three transmission lines, leading to six voltage dips over a two-minutes period. Nine wind farms reduced their active power production, as their control system was not able to withstand the voltage dips sequence. The imported power towards

SA quickly grew, with a consequent overload trip of the interconnection with a neighboring region. The load shedding protections in the SA area failed to trip, due to the too fast decay of the frequency, as it can be noted from Figure 1.2.

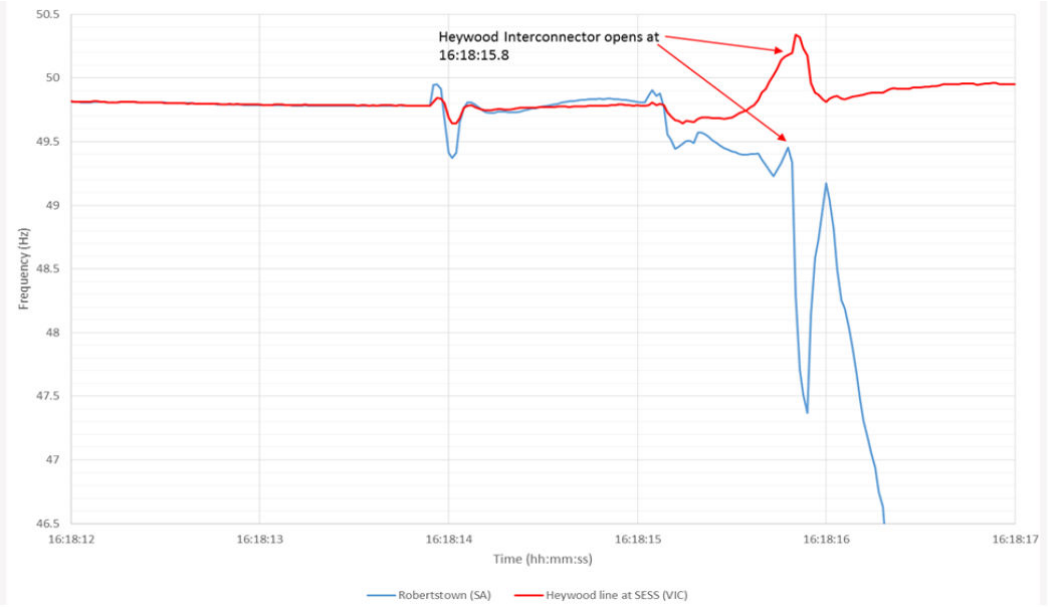

Figure 1.2: Frequency profile after SA grid separation. Source: [6].

The SA power system was therefore islanded from the rest of the system and the power imbalance led to the SA blackout. Two main conclusions can be deduced from this event:

1. A larger inertia is needed to reduce the RoCoF. This choice would facilitate the intervention of the protection relays;
2. Additional control systems are necessary to make RES plants withstand multiple fault events, so that they can contribute to the frequency regulation even after grid faults.

To solve these issues, according to the latest grid codes and pilot projects drafted by several Transmission System Operators (TSOs), the RPGs will be requested to provide ancillary services (i.e., inertial behavior, reactive support, harmonic compensa-

tion) as well [7, 8, 9, 10].

So far, it has been largely demonstrated that power electronic converters can perform these functions (e.g., droop control-based inverters for inertial support and frequency control [11], STATCOMs for reactive support, active filters for harmonic compensation [12]). A promising solution to provide all of them in a straightforward way is to make static converters behave as synchronous generators, guaranteeing inertial support, active and reactive power regulation as well as harmonic compensation. Many solutions have been proposed during the last 15 years, under the concept of Virtual Synchronous Generator (VSG) [13, 14], making difficult the selection of the most proper one.

The technical literature contains many different VSG solutions and therefore several survey papers have been proposed [13, 14, 15]. These survey papers adopted a pure descriptive approach of the available solutions, without neither simulation nor experimental comparison. Therefore, this paper represents a step forward as it allows a critical comparison based on experimental validation using the same setup and tuning criteria for all considered solutions. As a result, a benchmarking of the VSG solutions is possible to provide a useful tool for both researchers and application engineers when leveraging VSG technology in energy conversion. The inertial behavior and the frequency control capabilities of the VSGs are discussed and experimentally validated to provide a complete overview on the main features of each model. The goal is not to identify the best solution, but to show how the models behave in the field of application. The following ten VSG models available in the literature have been studied: Virtual Synchronous Machine (VISMA) [16, 17], VISMA I [18], VISMA II [19], Synchronverter [15, 20, 21, 22, 23], Osaka [24, 25], Synchronous Power Controller (SPC) [26, 27, 28, 29], VSYNC [30, 31], Kawasaki Heavy Industries (KHI) [32, 33], Cascaded Virtual Synchronous Machine (CVSM) [34, 35] and Simplified Virtual Synchronous

Compensator (S–VSC) [36, 37].

The analyzed models have been chosen, as they are representative of the many solutions and variants proposed in the technical literature. Indeed, most of them can be included into these ten VSGs as they present several common traits to the analyzed ones [13].

This paper is organized as follows. Section 2 provides the theoretical description of two fundamental aspects for the purpose of this paper: virtual inertia and frequency control. Section 3 is dedicated to the general aspects of the implementation and the common tuning procedure of the VSG control algorithms. In Section 4 each VSG solution is theoretically described, with a focus on the active part. Section 5 presents the experimental comparison of the ten analysed solutions and describes the main issues faced during the experimental implementation. Finally, the conclusions are given in Section 6.

2. Virtual Inertia and Frequency Control

To better describe the active parts of the VSG models, the concepts of virtual inertia and frequency control are defined in the next subsections.

2.1. The role of inertia

Synchronous generators provide electrical power by converting the mechanical power of a prime motor. This prime mover rotates and drag the generator rotor imposing a speed ω. Working with per unit (pu) quantities is useful to have a better sensibility both on the parameters and on their effect, as well as to facilitate the comparison among the solutions. Therefore, the majority of the equations are expressed in per unit. The relationship describing the rotor dynamics, neglecting the losses, damping

terms and assuming $\omega \simeq 1\,\text{pu}$, is the swing equation [3]:

$$P_m - P_e = 2H\frac{d\omega}{dt} \tag{2.1}$$

where P_m is the mechanical power (pu); P_e is the electrical power (pu); ω is the rotor speed (pu); H is the inertia constant (s), defined as follows:

$$H = \frac{1}{2}J\frac{\omega_b^2}{S_b} \tag{2.2}$$

In (2.2) J is the moment of inertia (kg m^2), S_b is the base power (VA) and ω_b is the base rotor speed (rad/s).

If the damping effect is taken into account, the swing equation becomes (2.3):

$$P_m - P_e = 2H\frac{d\omega}{dt} + k_d\Delta\omega \tag{2.3}$$

where k_d is the damping factor (pu) and $\Delta\omega$ is the difference between the actual speed and its reference (pu).

In electric power systems, during steady state operating condition, the speed ω is constant and the electrical power P_e is equal to the mechanical one P_m. As soon as the load increases, conventional generators immediately provides the requested power P_e, by ceding part of their kinetic energy stored in the rotor. Then, the frequency control increases P_m so that the speed and the frequency come back to their steady state values.

This is the behavior of conventional SGs, having rotating parts. To emulate this process with VSGs, the swing equation must be reproduced, defining H as a virtual inertia coefficient. The electrical power keeps the same meaning, whereas the mechanical term becomes the electrical reference power. In this case, since no rotating parts are

involved in static converters, the inertial action is therefore defined as virtual or synthetic [38, 39, 40]. The advantage of this approach lies in the tuning of the inertia coefficient, as it can be chosen to the best value for the application or even modified online during the operation, whereas SGs are constrained to their physical value. As the grid frequency increases or decreases, VSGs must be able to either inject or absorb active power accordingly, similarly to SGs. This implies that it is not possible to exploit the source as with MPPT techniques, since a margin has to be guaranteed (e.g., with power curtailment strategies). To improve the management of the power flow, an energy storage system can be used [41, 42]. If the power plant only provides inertial support, the amount of energy involved for this service does not necessarily require an energy storage system. Moreover, during the VSG tuning procedure, the presence of a battery storage system can be taken into account by choosing its inertial constant as a function of the storage capacity [43].

On the other hand, in case of primary and secondary frequency regulation, the size of the storage system depends on the management strategy of the plant and any contractual arrangements with the TSO. An example is the pilot project "Fast Reserve" proposed by the Italian TSO, Terna [9], which requires selected companies to provide primary frequency regulation for an expected time of 1000 hours, therefore imposing a sizing criterion for the storage capacity.

2.2. Frequency Control

The frequency can be regulated according to a proportional droop control. In case of inductive lines, there is a close link between frequency and active power, shown in (2.4):

$$\frac{f - f_0}{f_0} = -b_p \frac{P - P_0}{P_0} \tag{2.4}$$

where f is the output frequency (Hz); f_0 is the rated frequency (Hz); b_p is the active droop coefficient; P is the output active power (W) and P_0 is the rated active power (W). Implementing this law into the control algorithm of a converter, this can provide the primary frequency control.

2.3. Distinction between damping and droop

The coefficient k_d is responsible to damp the electromechanical oscillations of the rotor. It is used by the VSGs based on (2.3) to provide the appropriate damping and its typical value is around 200–400 pu. On the other hand, the droop coefficient b_p is responsible of the primary frequency control and it has typical values around 0.05 ($1/b_p = 20$) [3]. Therefore, $1/b_p$ and k_d typically differ for one order of magnitude. In the following, it is illustrated that some VSG solutions inherently embed the active droop control, whereas the others have dedicated part to it. In the VSG models where the damping and droop are coupled, the droop coefficient cannot be tuned because $1/b_p \equiv k_d$, with a consequent droop coefficient 10 times lower than the conventional case. On the opposite, in the models where $1/b_p$ and k_d are two separate coefficients, b_p is set to 5%.

3. General Aspects of the VSG models

This Section provides general information about the system on analysis and the tuning procedure of the VSG models.

3.1. Scheme of the hardware on study

The reference hardware to study and implement the VSG solutions is shown in Figure 3.1.

This hardware consists of a dc voltage source, supplying a two-level three-phase inverter connected to the grid through an LCL filter. This filter is needed to limit the

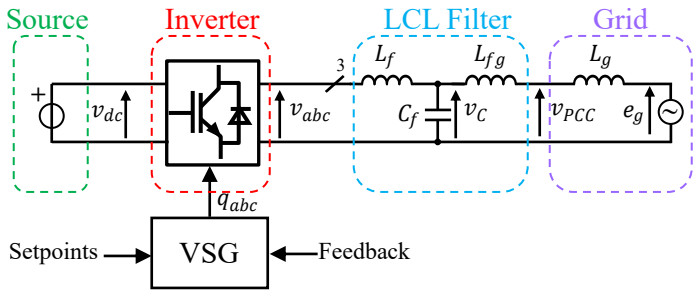

Figure 3.1: Hardware block diagram for the considered VSG solutions.

impact of the PWM harmonics content. The LCL filter is one of the most adopted solution to interface power converters to the electric grid [2]. It consists of an inverter-side inductor (inductance L_f), a filter capacitor (capacitance C_f) and a grid side inductor (inductance L_{fg}). The grid is modelled as a Thévenin equivalent circuit, with a grid inductance L_g. The VSG block contains the whole control algorithm, including a Phase Locked Loop (PLL) used to synchronize the inverter with the grid [2], the Pulse Width Modulation (PWM) and the analog acquisition. The Point of Common Coupling (PCC) defines the connection between the inverter and the grid. The voltage measured for the control algorithms is v_C.

3.2. Current Source and Voltage Source VSGs

The VSG models can be gathered into two main categories: current source and voltage source.

current source VSG models provide as output the current reference i^*_{abc}. The equivalent circuit is depicted in Figure 3.2.

The current reference i^*_{abc} can be retrieved as the product of the difference between the virtual electromotive force e_{abc} of the VSG and the phase voltage v_C and a virtual admittance. This is arbitrary tunable by defining a virtual resistance R_v (r_v in pu) and a virtual inductance L_v (l_v in pu). Their values have been chosen according to the typical values of synchronous generators [3] and are 0.02 pu and 0.1 pu, re-

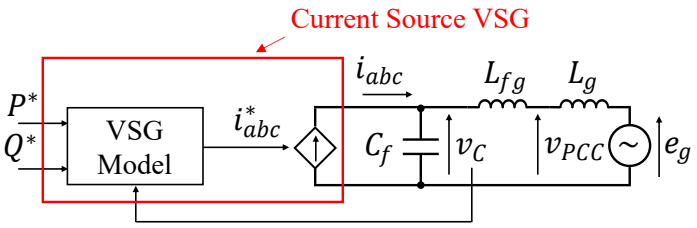

Figure 3.2: Equivalent circuit of current source VSGs.

spectively. Then, a closed loop current control is implemented to retrieve the voltage references which are used to obtain the commands for the inverter, according to the PWM algorithm. In this paper, the control is performed by means of a conventional PI regulator in the (d, q) reference frame, tuned according to technical literature [2]. On the other hand, in voltage source VSG models, the voltage references are the electromotive forces e_{abc} produced by the VSG algorithm and they are directly provided to the PWM Modulator, without using an inner controller. The equivalent circuit is proposed in Figure 3.3. This open loop voltage control does not embed a current saturation system. Therefore, during the testing phase, it may result in an overcurrent protection of the converter. For this reason, backup strategies must be implemented to preserve the operation of the converter even during faulty conditions.

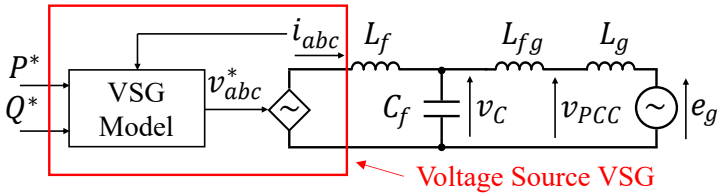

Figure 3.3: Equivalent circuit of voltage source VSGs.

3.3. Common Tuning Procedure

To tune the parameters of VSGs, a common linearised model (in per unit) is described in this subsection. It is then applied to the considered models.

The connection between a generic voltage source (like the VSG equivalent stator) and the grid can be represented with the circuit shown in Figure 3.4.

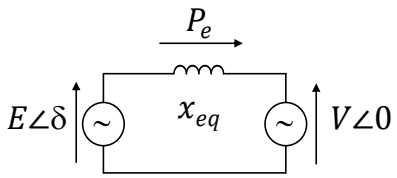

Figure 3.4: Simplified circuit of connection between VSG stator and grid for active control tuning.

This representation is valid for the systems where the resistive term is negligible compared to the inductive one (e.g., high voltage lines) [3]. The quantities of this model, in per unit, are: $V\angle 0$, the grid voltage expressed in the polar notation (pu); $E\angle\delta$, the VSG electromotive force voltage (pu); x_{eq}, the equivalent reactance between the two voltage sources (pu); P_e, the active power transferred from one side to another, expressed in per unit:

$$P_e = \frac{EV}{x_{eq}} \sin(\delta) = K_s \sin(\delta) \tag{3.1}$$

where K_s is the synchronizing power (pu), equal to the theoretical maximum transferable power between the two voltage sources [3].

The equivalent reactance X_{eq} (Ω) is given by the sum of three terms:

$$X_{eq} = \omega_b(L_s + L_{fg} + L_g) \tag{3.2}$$

where L_g is the grid inductance (H); L_{fg} is the grid-side filter inductance (H); L_s is the VSG inductance (H). For voltage source models it is equal to the real filter inductance L_f, whereas, for current source models, it is equal to the virtual inductance L_v, located inside the VSG Model block of Figure 3.2.

As it has been demonstrated in the technical literature, weak grids can compromise the performance of current source VSGs [44]. To mitigate the negative effect of weak

grids, this tuning procedure includes the estimation of the grid inductance L_g.

By defining the base impedance Z_b (Ω) as the ratio between the base voltage V_b (V) and the base current I_b (A), the equivalent reactance x_{eq} (pu) can be retrieved from (3.2):

$$x_{eq} = \frac{X_{eq}}{Z_b} = \frac{\omega_b}{Z_b}(L_s + L_{fg} + L_g) = l_s + l_{fg} + l_g = x_s + x_{fg} + x_g \tag{3.3}$$

where l_g and x_g are respectively the grid inductance and reactance (pu); l_{fg} and x_{fg} are respectively the grid-side filter inductance and reactance (pu); l_s and x_s are respectively the VSG inductance and reactance (pu).

Considering a small deviation (denoted by the prefix Δ) from the nominal working point, (3.4) and the linearised model in Figure 3.5 can be retrieved by means of (2.3) and (3.1), as demonstrated in [3].

$$\Delta P_e = K_s \sin(\Delta\delta) \simeq K_s \Delta\delta \tag{3.4}$$

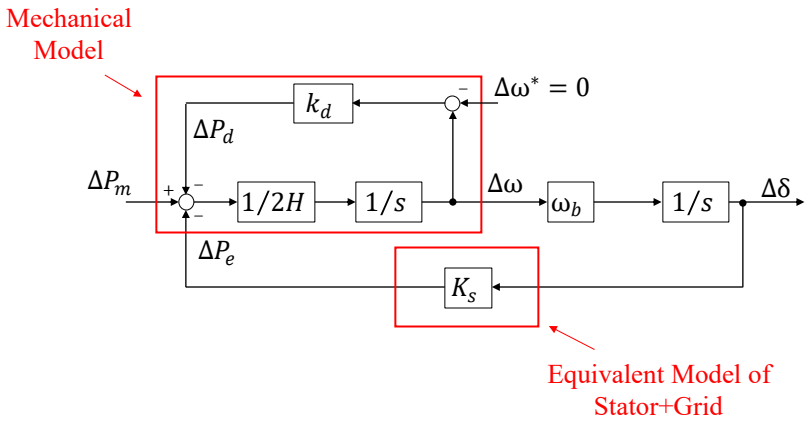

Figure 3.5: Linearised model in per unit of VSG stator connected to the grid.

Then, the characteristic equation of the system in Figure 3.5 can be obtained (3.5a) and compared with the general characteristic equation for a second order system

(3.5b):

$$\begin{cases} s^2 + \dfrac{k_d}{2H}s + \dfrac{\omega_b K_s}{2H} = 0 & \text{(3.5a)} \\ s^2 + 2\zeta\omega_N s + \omega_N^2 = 0 & \text{(3.5b)} \end{cases}$$

In (3.5b), ζ is the desired damping factor and ω_N is the natural frequency (rad/s) of the system. The results, useful for some VSG solutions, can be obtained from the comparison of (3.5a) and (3.5b):

$$\begin{cases} k_d = 2\zeta\sqrt{2H\omega_b K_s} & \text{(3.6a)} \\ \omega_N = \sqrt{\dfrac{\omega_b K_s}{2H}} & \text{(3.6b)} \end{cases}$$

In some cases, the frequency ω_{PLL} retrieved by the PLL is used instead of the reference ω^*. In this circumstance, the linearised model changes and k_d must be multiplied times a correction factor k_c [45]:

$$\begin{cases} k_c = \dfrac{L_s + L_{fg} + L_g}{L_s} & \text{(3.7a)} \\ k'_d = k_d k_c & \text{(3.7b)} \end{cases}$$

The damping factor ζ and the inertia constant H are set to typical values [3], whereas the synchronizing power K_s depends on the equivalent reactance x_{eq}. These values, together with the base values, the results of the tuning and the parameters for the current and voltage source models are listed in Table 3.1.

To provide a fair comparison between the VSG solutions, it has been decided to use the same design parameters (i.e., inertia constant, virtual stator inductance, damping factor...) for each of them. In this way, the peculiarities of each model can be evaluated and compared fairly. The optimization of each control algorithm is out of the scope of this paper, as it would only marginally affect the performance of each solu-

Base Values		Common Parameters		Current Source Parameters		Voltage Source Parameters	
S_b	15 kVA	V	1 pu	l_v	0.1 pu	l_f	0.059 pu
V_b	$120\sqrt{2}$ V	E	1 pu	x_{eq}	0.146 pu	x_{eq}	0.105 pu
I_b	60 A	l_{fg}	0.013 pu	K_s	6.85 pu	K_s	9.5 pu
Z_b	2.88 Ω	l_g	0.033 pu	k_d	184 pu	k_d	216 pu
f_b	50 Hz	ζ	0.7	ω_N	16.40 rad/s	ω_N	19.31 rad/s
ω_b	314 rad/s	H	4 s	k_c	1.46 pu	k_c	1.77 pu
				k'_d	269 pu	k'_d	383 pu

Table 3.1: Parameters for VSG tuning.

tion, while keeping intact the core behavior and features of each model.

4. Description of the VSG models

This Section is dedicated to the description of each VSG model considered in this paper. The analyzed VSG solutions have been implemented according to the original structure of their corresponding papers, with no modifications. However, to obtain a fair comparison on the same setup, the paper proposes a common parameter tuning procedure, described in subsection 3.3. Finally, the nomenclature is common among the models to facilitate the description and the comparison, unless specific symbols are required.

4.1. VISMA

VISMA is the first VSG model proposed in 2007 [16, 17]. The general structure is shown in Figure 4.1.

This solution fully emulates the behavior of a synchronous generator. In fact, it is implemented using the complete electromechanical model of a SG. It is a current source model. It creates the current references in the (d, q) reference frame by means of the synchronous generators equations [17]. The mechanical part contains (2.1).

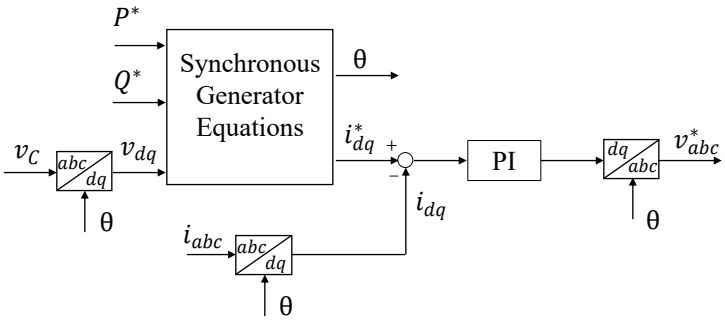

Figure 4.1: VISMA control scheme in Laplace domain [17].

4.2. VISMA I

VISMA I is a simplified version of VISMA, proposed in 2011 [18]. The control block scheme of the model is depicted in Figure 4.2.

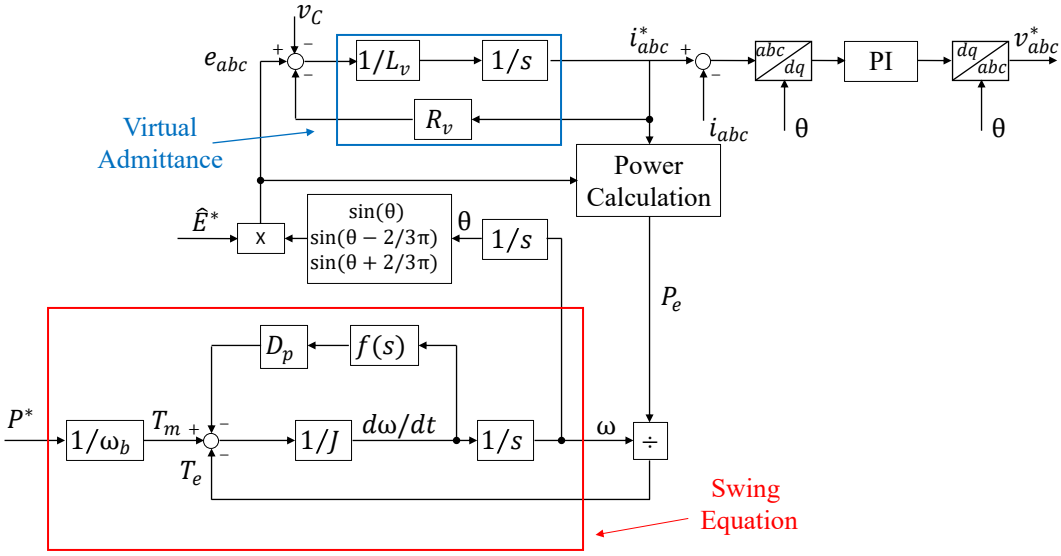

Figure 4.2: VISMA I control scheme in Laplace domain [18].

The VISMA I is a current source model. The active part is expressed in terms of torque and it shows a slight difference with respect to (2.3):

$$T_m - T_e = J\frac{d\omega}{dt} + D_p f(s)\frac{d\omega}{dt} \tag{4.1}$$

where T_m is the mechanical torque (Nm), which emulates the mechanical torque of a

primary motor for conventional SGs; T_e is the virtual torque of VISMA I (Nm); $f(s)$ is the phase compensation term, a first order low pass filter.

4.3. VISMA II

VISMA II is the second simplified version of VISMA, proposed in 2012 [19]. Its control scheme is proposed in Figure 4.3.

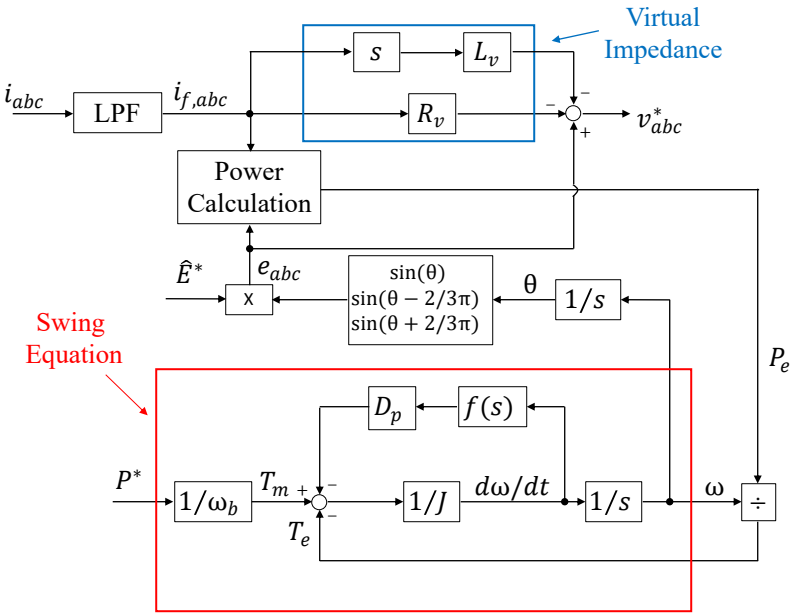

Figure 4.3: VISMA II control scheme in Laplace domain [19].

Differently from VISMA and VISMA I, VISMA II is a voltage source model. Consequently, a backup strategy is needed to prevent overcurrent faults. The active part is the same of VISMA I. The current derivative calculus implies the use of a low pass filter (LPF).

4.4. Synchronverter

The Synchronverter was proposed for the first time in 2009 [20] and then it has been improved up to reach the version illustrated in Figure 4.4 [23, 15].

It is a current source model and it can synchronize with the grid without using a PLL.

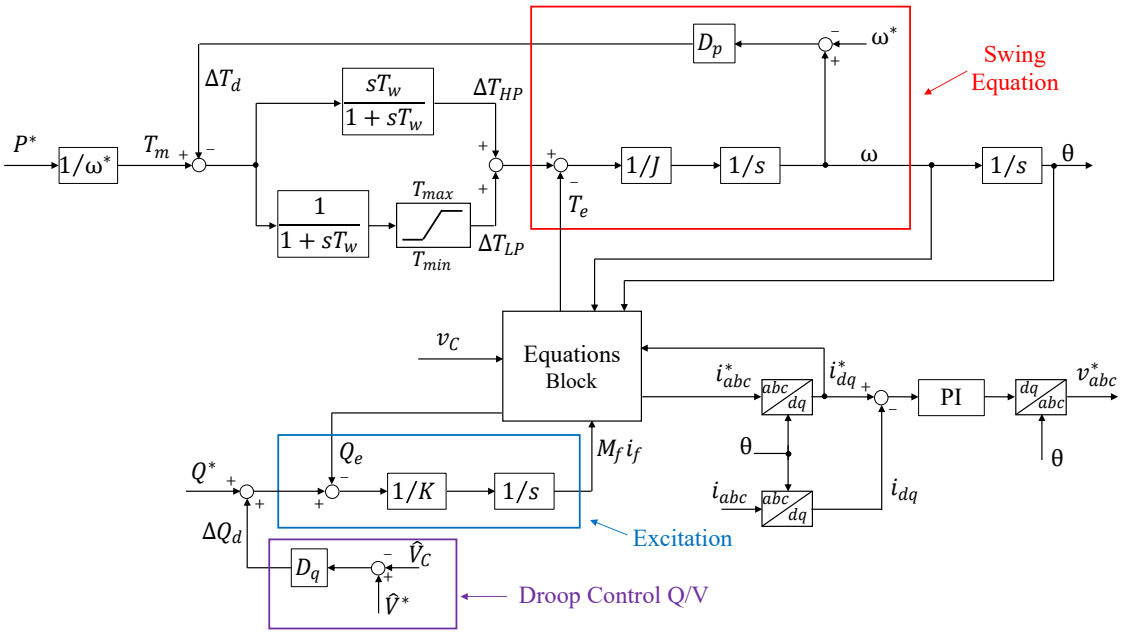

Figure 4.4: Synchronverter control scheme in the Laplace domain [23].

The active part is based on (2.3) written in terms of torque (Nm):

$$T_m - T_e = J\frac{d\omega}{dt} + D_p(\omega - \omega^*) \tag{4.2}$$

where T_m is the fictitious mechanical torque of the virtual generator (Nm), obtained from the ratio between the active power reference P^* (W) and the reference speed ω^* (equal to ω_b); D_p is the damping factor $\left(\text{kg}\frac{\text{m}^2}{\text{s}}\right)$.

4.5. Osaka

Osaka model is a solution proposed in 2011 [24, 25]. Its control scheme is depicted in Figure 4.5. It is a voltage source model. A governor model is used to actuate the primary regulation of the frequency. It is characterised by the droop coefficient b_p and a low pass filter. Then, the internal active power reference P_{in} (pu) is computed, taking the influence of the voltage variability into account:

$$P_{in} = \widehat{V}_C^2(P_\omega + P^*) \tag{4.3}$$

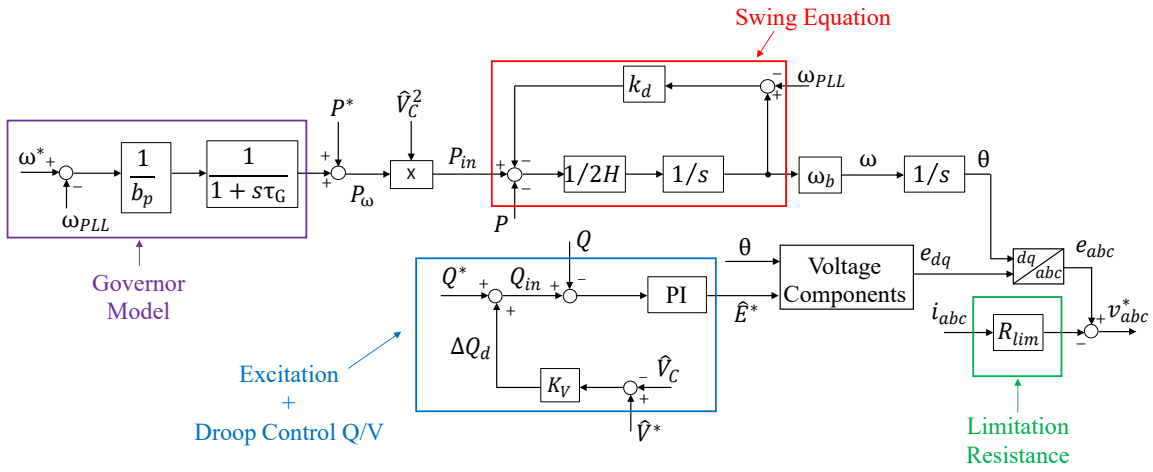

Figure 4.5: Osaka control scheme in Laplace domain [24].

where P^* is the active power reference (pu) and $\widehat{V_C}$ is the voltage amplitude on the capacitors (pu). A limitation resistance R_{lim} can be arbitrary tuned to limit the current in case of faulty conditions. Nevertheless, a backup strategy is needed to avoid overcurrent faults.

4.6. SPC

The SPC is a current source model proposed in 2011 [26, 27, 28, 29]. Its control block scheme is shown in Figure 4.6.

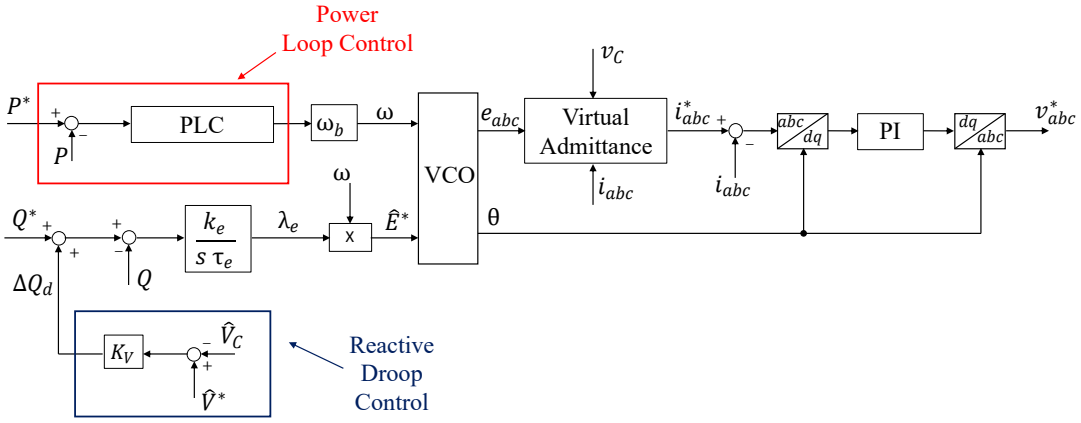

Figure 4.6: SPC control scheme in Laplace domain [27].

SPC is a self–synchronizing model that autonomously synchronizes with the grid,

avoiding any PLL. The Power Loop Controller (PLC) is used to retrieve the SPC speed ω. Three different versions of SPC have been proposed: SPC–SG, SPC–PI and SPC–LL. The difference among them lies in the PLC transfer function, as follows (in per unit):

$$\begin{cases} PLC_{SG}(s) = \dfrac{S_b}{\omega_b}\dfrac{k\omega_c}{s+\omega_c} & \text{(4.4a)} \\ PLC_{PI}(s) = \dfrac{S_b}{\omega_b}\dfrac{k_p^{PI}s + k_i^{PI}}{s} & \text{(4.4b)} \\ PLC_{LL}(s) = \dfrac{S_b}{\omega_b}\dfrac{k_p^{LL}s + k_i^{LL}}{s+k_g} & \text{(4.4c)} \end{cases}$$

4.7. VSYNC

The VSYNC was proposed in 2009 [31]. Its control scheme in the Laplace domain is illustrated in Figure 4.7.

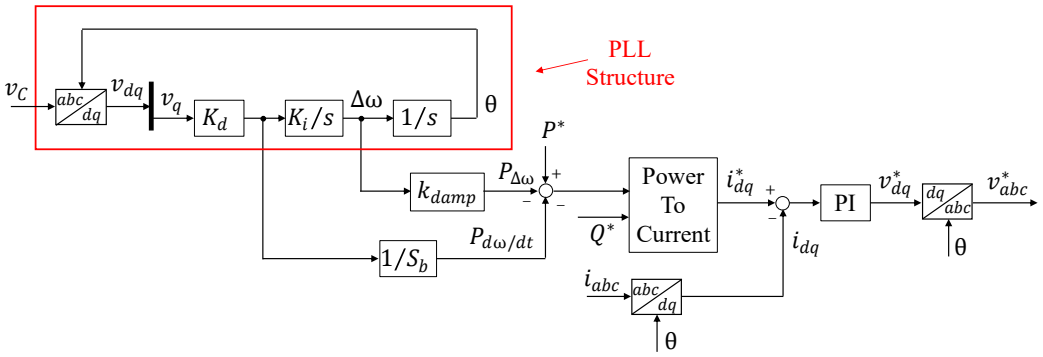

Figure 4.7: VSYNC control scheme [31].

VSYNC is a current source model. Its core has a structure very similar to a PLL one, highlighted in red in Figure 4.7. This allows the synchronization with the grid with no other elements. Moreover, from the strict analogy between the PLL structure and the swing equation, the coefficients K_d and K_i can be defined [31]:

$$\begin{cases} K_d = \dfrac{3}{2}\dfrac{V_b}{X_{eq}} & \text{(4.5a)} \\ K_i = \dfrac{\omega_b}{2HS_b} & \text{(4.5b)} \end{cases}$$

No active and reactive power loop control are used.

4.8. Kawasaki Heavy Industries

KHI (Kawasaki Heavy Industries) was proposed in 2012 [32, 33]. The block scheme is illustrated in Figure 4.8.

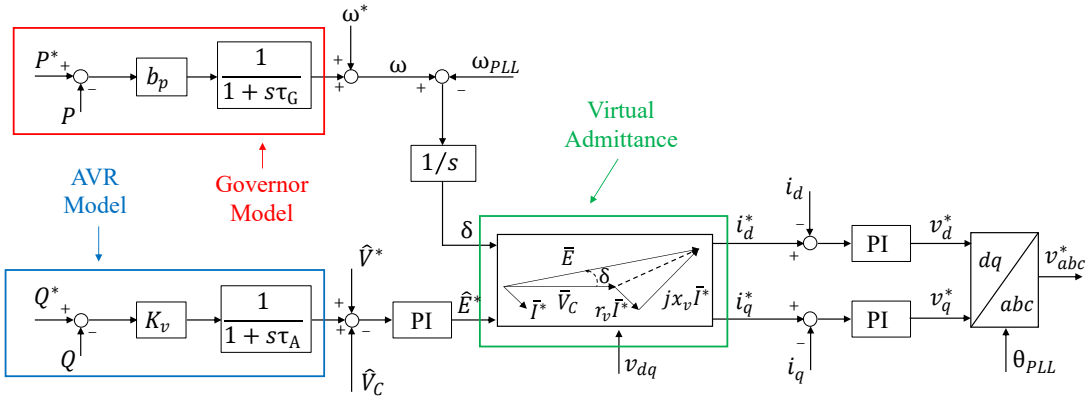

Figure 4.8: KHI control scheme in Laplace domain [32].

KHI is a current source model. The model of a virtual governor is used to perform an active droop control, characterized by the droop coefficient b_p and a low pass filter. The electromotive force e_{abc} and the phase voltage v_C are here represented as the vectors $\overline{E}$ and $\overline{V}_C$, respectively. The phase angle between them, indicated with δ, is retrieved by means of the governor and the PLL frequency ω_{PLL}. The KHI model uses the concept of the virtual admittance to retrieve the current reference i^*_{dq}, as the other VSG solutions. However, here, the virtual admittance is algebraically implemented [32].

4.9. Cascaded Virtual Synchronous Machine

The CVSM (Cascaded Virtual Synchronous Machine) is a current source model proposed in 2013 [34, 35]. The general block scheme is illustrated in Figure 4.9.
The active part of the model is divided into two parts: Power Control and Virtual Inertia. The former is used to actuate the active droop control. The latter embeds the

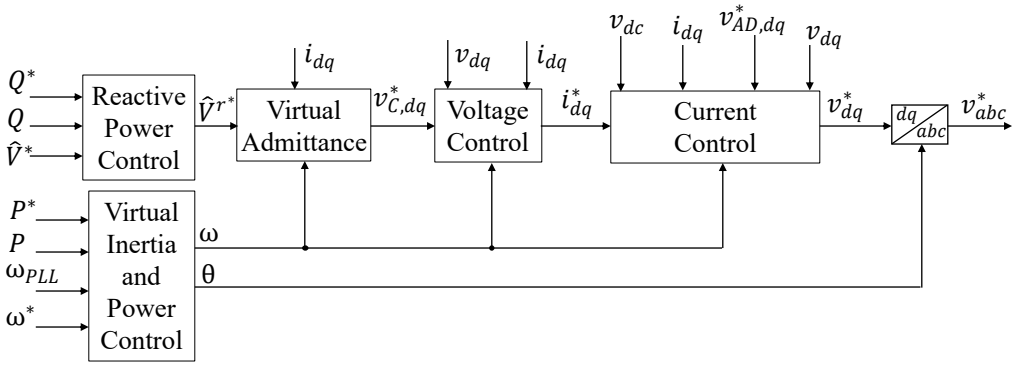

Figure 4.9: CVSM control scheme [34].

conventional swing equation seen in (2.3). CVSM does not need PLL to synchronize with the grid, but a PLL is needed to damp the electromechanical part [35].

The core of the CVSM model is constituted by two cascaded voltage and current controllers in the (d, q) reference frame, tuned according to [46]. The implementation of the virtual admittance is simplified, by neglecting the terms proportional to the current derivatives.

4.10. Simplified Virtual Synchronous Compensator

The S–VSC (Simplified Virtual Synchronous Compensator) is a current source model [36, 37]. The block scheme is illustrated in Figure 4.10.

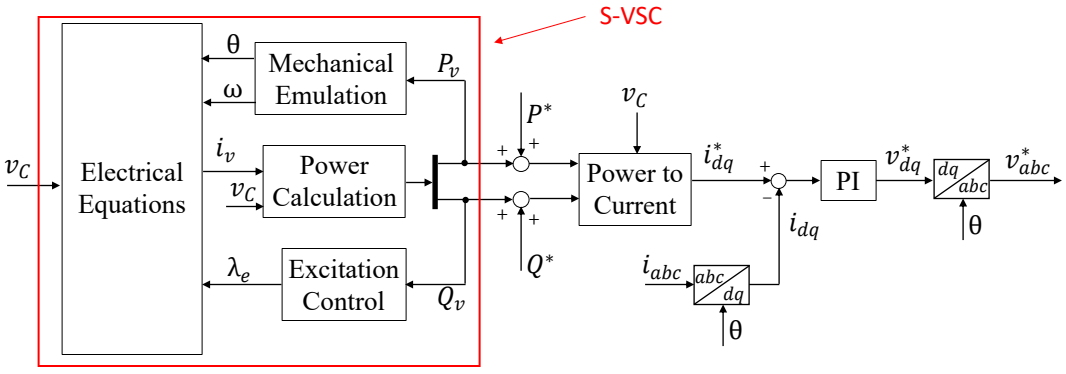

Figure 4.10: S–VSC control scheme [36].

The Mechanical Emulation block contains (2.1). The core of the model is the Electrical Equations block, which embeds modified equations of the electromagnetic model

of synchronous generators [36]. The damping of the S–VSC is performed by means of an equivalent q–axis damper winding. This choice guarantees a full decoupling between the damping and the primary frequency control. The references P_v and Q_v are used only to provide ancillary services and the inverter control is performed by means of the external references P^* and Q^*.

5. Experimental Comparison

In this Section, the results of the experimental tests are provided together with comments on the main experimental implementation aspects.

5.1. Experimental Setup and Tests

The experimental setup used for the tests is depicted in Figure 5.1a. It consists of: a dc source; a three phase inverter controlled by dSPACE according to the VSG algorithms; an LCL filter, which interfaces the inverter with the grid emulator; a grid emulator, used to create an ideal three phase voltage to emulate the grid and simulate frequency and voltage variations. The diagram of the experimental setup is displayed in Figure 5.1b. The main data are summarised in Table 5.1.

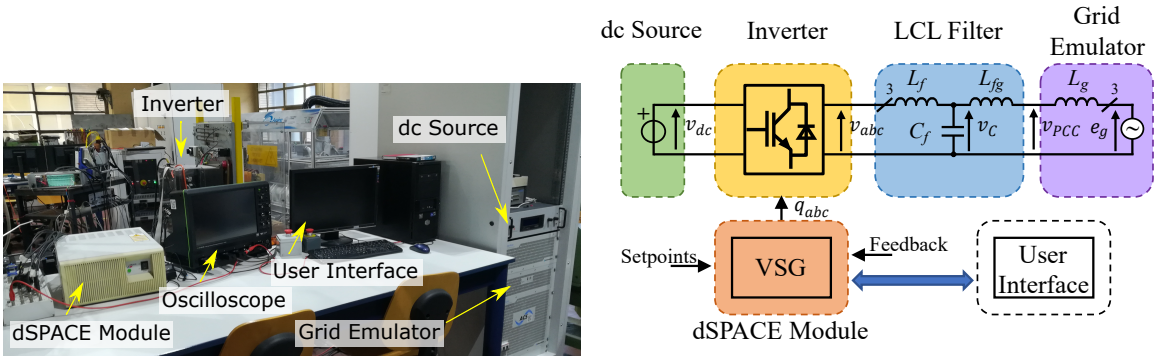

(a) (b)

Figure 5.1: From left to right: (a) Picture of the experimental setup; (b) Diagram of the experimental setup.

dc Source		Inverter		LCL Filter		Grid Emulator	
V_{dc}	380 V	S_N	15 kVA	L_f	545 µH	$\widehat{E}_g$	$120\sqrt{2}$ V
		I_N	60 A	C_f	22 µF	f_g	50 Hz
		f_{sw}	10 kHz	L_{fg}	120 µH	L_g	300 µH

Table 5.1: Main data of the experimental setup.

This paper proposes an experimental comparison among the VSG solutions considered in this paper, with a special focus on the active part. Therefore, two tests have been performed. In both tests the power converters are connected to an emulated grid, where the frequency and the voltage are imposed.

Test 1: Active power reference step from 0.3 pu to 0.4 pu. This test shows the dynamic behavior of the considered VSG models if requested to change their power set-point, such in case of a variation of the power generated by a renewable energy source connected to the dc side of these converters. This test was implemented to analyze the dynamic performance of the control algorithm.

Test 2: Large power imbalance emulation. The grid frequency varies following a profile similar to the qualitative one displayed in Figure 1.1b and settles to the final value of 49.58 Hz. This is the typical frequency trend which occurs when a generation source is lost. Test 2 is useful to analyse three different aspects:

1. *Inertial behavior*: as described in Section 1, when a power imbalance occurs, the SGs provides part of their kinetic energy to compensate it. By means of this test, the capability of VSGs to emulate this feature is evaluated;
2. *Active droop control*: it is the second step of the profile in Figure 1.1b. It is an additional feature of some models, whereas others inherently embed it. The Test 2 shows how they perform the primary frequency control;
3. *Damping-droop coupling*: as mentioned before, some models show a coupling between the damping coefficient and the droop one, while others do not. This

test can be used to evaluate this characteristic.

5.2. Test 1: Active Power Reference Step

Figure 5.2 shows the results of Test 1 for each model. The active power reference varies from 0.3 pu to 0.4 pu. The models have been grouped according to the time needed to reach the steady state condition.

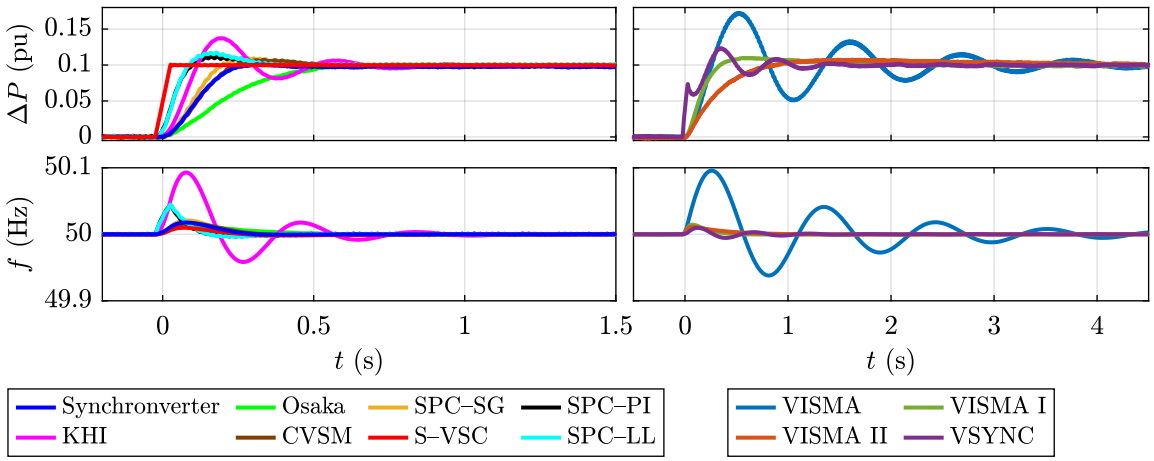

Figure 5.2: Results of Test 1: (top) moving average of the active power variation (pu) ΔP injected by the inverter; (bottom) corresponding frequency f profile (Hz).

For each VSG model the active power tracks the reference with no steady state error. Most of them show a high quality response in terms of settling time and damping. The S–VSC model shows the fastest response among the solutions, with no overshoot. As the virtual active power P_v of the S–VSC is little modified, the response only depends on the current loops dynamics and there is no virtual mechanical transient and load angle variation. Therefore, the frequency profile is characterised by the smallest variation among the models.

For Osaka and VISMA II solutions the profile is damped, whereas for Synchronverter, VISMA I, the three SPC versions and CVSM the response is underdamped or with a limited overshoot. In all these cases the setpoint is reached in at most 1 s. As regards the frequency variation, in almost all cases it does not overcome the value of 20 mHz.

The exceptions are SPC–PI and SPC–LL, with a maximum value of circa 60 mHz, due to the presence of a proportional gain.

VISMA, VSYNC and KHI models presents a consistent underdamped profile. Obviously, VISMA shows the highest overshoot and settling time, because it fully emulates conventional synchronous generators, characterized by low damping.

As regards the VSYNC and KHI solutions, in both cases the response is underdamped and the transient ends after circa 1.5 s. A difference lies in the frequency variation: for VSYNC it is about 10 mHz, much lower than the value of 100 mHz reached by KHI, the highest value of frequency variation among the solutions.

5.3. Test 2: Large Power Imbalance Emulation

The results of Test 2 are illustrated in Figure 5.3. The grid frequency varies with an initial RoCoF of about -0.89 Hz/s, reaches a nadir around 48.65 Hz and settles to the final value of 49.58 Hz. As already stated in Section 4, the VSG models are compared with no alteration of the original control algorithm. They can be gathered into three groups:

- Models which show a coupling between the damping and the droop: VISMA I, VISMA II, Synchronverter and SPC–SG. See Figure 5.3 on the right;
- Models with an embedded droop control, in which the damping and the droop control are decoupled: Osaka, SPC–PI, SPC–LL, KHI and CVSM. See Figure 5.3 on the left;
- Models without an embedded droop control, which can be easily added externally, if needed: VISMA, VYSNC and S–VSC. See Figure 5.3 on the left.

Almost all models are based on an active power loop control. The active power (or torque) used as feedback is either measured (real active power injected by the model,

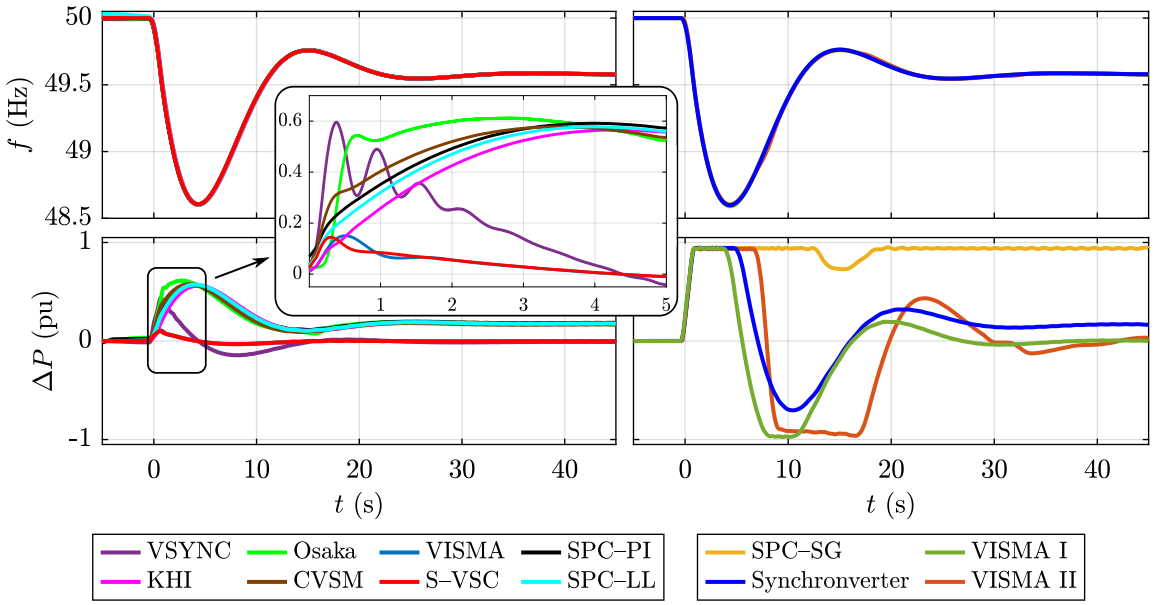

Figure 5.3: Results of Test 2: (top) frequency f profile of each VSG solution, varying from 50 Hz to 49.58 Hz; (bottom) moving average of the active power variation ΔP (pu) of each VSG solution.

indicated here as P) or calculated (virtual active power, indicated here as P_v) according to the model. Independently on this, they coincide as long as the injected active power is not limited. If it saturates, the virtual power must be calculated with no limitation to guarantee the stability of the control. Then, the algorithm takes charge to limit the current. In the group on the left in Figure 5.3, the virtual active power does not reach values larger than 1 pu because damping and droop are not coupled. The damping term is in charge of damping the oscillation (if present) and the droop coefficient defines the injected active power in steady state (if present). Conversely, the group on the right gathers the VSG models in which the virtual active power exceeds the nominal value because the damping and the droop are coupled. In this case, the droop coefficient is correlated to the damping one. In all cases, the real active power injected by the inverter must be saturated to comply with the inverter rating. Figure 5.4 shows the active power before and after the saturation.

It can be observed that each model, independently on the employment of a PLL, per-

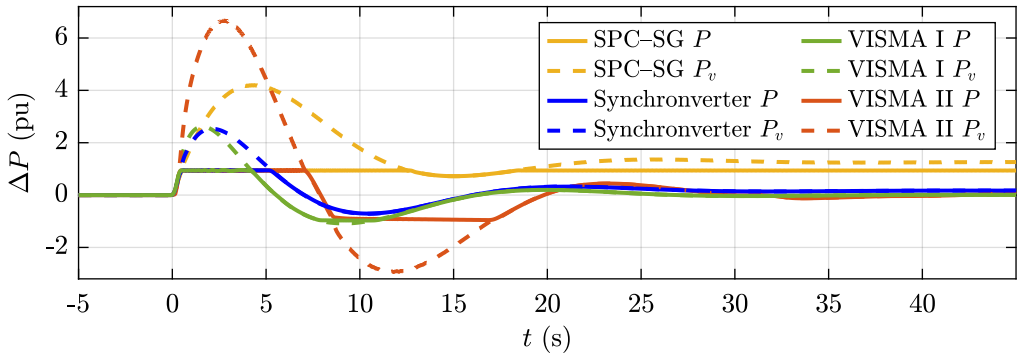

Figure 5.4: Results of Test 2: Comparison between the real active power P injected by VISMA I, VISMA II, Synchronverter and SPC–SG and the corresponding virtual active power P_v.

fectly tracks the grid frequency. In the first instants, the VSG models show the typical inertial behavior of the conventional SGs and inject inertial active power, proportional to the inverse of the frequency derivative. In the subsequent seconds, the responses strongly depend on how the active droop control is implemented.

Osaka, SPC–PI, KHI and CVSM models use a governor model to regulate the frequency. In steady state, by setting the droop coefficient to the conventional value of 5%, these VSGs inject the same active power, equal to 0.168 pu. During the transient, the SPC–PI and KHI show circa the same behavior.

As regards the response of the Osaka model, the active power trend shows a higher slope with respect to the other three models just described. Since it is a voltage source model, its damping coefficient is higher than the current source model one, as can be observed from Table 3.1. In the first instants, the damping coefficient amplifies the frequency difference and gives its contribution together with the governor. The higher is the damping coefficient, the higher is the active power peak. In fact, in this case the active power peak is about 0.6 pu.

Finally, even the CVSM solution shows a faster dynamic compared to SPC–PI and KHI. Here, the reason is the lack of a low pass filter in the frequency controller. There is only a gain corresponding to the droop coefficient of 5%. The active power peak is

around 0.6 pu.

Then, Synchronverter and SPC–LL models do not embed a dedicated governor, but still can inject active power after a grid frequency variation. During the first instants, the former shows a virtual active power peak of 2.5 pu, since high pass term ΔT_{HP} is not saturated. In steady state, this term is zero and the only contribution comes from ΔT_{LP}. It is limited to 0.168 pu, the maximum transferable active power with a droop coefficient of 5%.

The SPC–LL shows a peculiar behavior: the active power trend is the same of SPC–PI and KHI, even if there is no dedicated governor model. The reason lies in the structure of lead–lag PLC. There is, in fact, an additional degree of freedom [27] which can be used to decouple the damping effect and the droop control. The frequency control is an embedded but tunable feature of this solution.

Concerning VISMA, VISMA I, VISMA II, SPC-SG, VSYNC and S–VSC models, they do not implement a governor. Therefore, these solutions do not actuate a primary frequency control. Nevertheless, an external droop controller can be added. VISMA completely emulates the behavior of a synchronous generator. The active power trend in this case is much lower than the others. The peak is 0.1 pu. At steady state, the active power is zero because no governor is implemented. A very similar response is given by the S–VSC, whose control scheme has many aspects in common with the VISMA one.

For VISMA I, VISMA II and SPC–SG models the virtual active power grows overcoming the limit of 1 pu during the first part of the frequency variation. Then, at steady state, the active power of VISMA I and VISMA II goes to zero because of the lack of a frequency controller. On the contrary, the SPC–SG injects the maximum active power during all the time, because of the coupling between the droop and the damping coefficient. In fact, the droop coefficient is constrained by the damping one

and it is circa 10 times lower than the other cases. This leads to inject more active power with respect to the other models (e.g., SPC–PI and SPC–LL).

Finally, the VSYNC solution does not embed an active power loop. The active power is measured and it is not used as feedback. When the frequency variation occurs, the VSYNC active power grows and starts to oscillate. At steady state active power goes to zero because of the lack of a governor model.

5.4. Experimental implementation aspects

The VSG algorithms and their tuning have been first verified by means of PLECS simulations. Next, they have been implemented on the experimental setup. Some challenging issues arose in this phase:

- *Synchronization procedure*: the converter must synchronize to the grid without inrush currents. Typically, this is done with a PLL algorithm or other techniques. These are not suitable for the SPC and the KHI models because they employ the measured powers as feedback in their active power loops. Therefore, to synchronize them to the grid, the power must be first calculated with the current references. Then, when the synchronization is complete, the control is restored to the original configuration, using the measured power.

- *Current Limitation*: the voltage source models (i.e., VISMA II and Osaka) do not embed a current limitation algorithm. Therefore, a backup strategy was implemented to guarantee the safe operation of the inverter. As soon as a current threshold is exceeded, the inverter switches to a current source operation to easily limit the current. Then, when a safe condition is reached, the original control algorithm is restored. This transition can be noted for VISMA II in Figure 5.3 at 32 s.

Another issue related to the limitation of current regards again the SPC and the KHI models, which use the measured power as feedback. When the current reference is saturated to avoid faults, they must switch to calculated power feedback with no saturated current reference. Otherwise, the control diverges.

6. Conclusions

Virtual Synchronous Generators represent a promising solution to facilitate the spread and the penetration of the renewable energy plants into the electrical system. Indeed, by means of this control approach, renewable power generators can provide ancillary services, guaranteeing the grid frequency stability.

In this paper, ten VSG solutions available in the literature have been analyzed and compared under the same tuning procedure. Then, two kinds of experimental tests have been actuated to show how VSGs work on the field of application, to highlight their main peculiarities.

Test 1 verifies the dynamic properties of the active parts, by means of a power reference step variation. Only VISMA and KHI show a no satisfying behavior, because of their consistent overshoots.

Test 2 evaluates their inertial behavior, as well as their capability to actuate frequency control. Both are essential features for the grid correct operation. Synchronverter, Osaka, SPC–SG, SPC–PI, SPC–LL, KHI and CVSM can actuate the primary frequency regulation. However, in the SPC–SG model the droop coefficient depends on the damping term. For the remaining models, the droop control can be included as an additional feature with tunable parameters. The experimental results of the ten VSG solutions are summarised in Table 6.1. The three versions of the SPC are displayed separately. The final column entitled “Implementation Aspects” summarizes the main experimental implementation aspects, discussed in 5.4: synchronization pro-

cedure and current limitation.

Model	Active Power Reference Step		Frequency Variation		Implementation Aspects
	Damping	Frequency Peak	Damping–Droop Decoupling	Tunable Droop	
VISMA	✘	✘	✔	✔	✔
VISMA I	✔	✔	✘	✔	✔
VISMA II	✔	✔	✘	✔	✘
Synchronverter	✔	✔	✘	✔	✔
Osaka	✔	✔	✔	✔	✘
SPC–SG	✔	✔	✘	✘	✔
SPC–PI	✔	✘	✔	✔	✔
SPC–LL	✔	✘	✔	✔	✔
VSYNC	✘	✔	–	✔	✔
KHI	✘	✘	–	✔	✘
CVSM	✔	✔	✔	✔	✘
S–VSC	✔	✔	✔	✔	✔

Table 6.1: Results of the comparison.

Funding: This research did not receive any specific grant from funding agencies in the public, commercial, or not-for-profit sectors.

References

[1] International Energy Agency, Electricity generation by fuel and scenario, 2018-2040.

[2] R. Teodorescu, M. Liserre, P. Rodriguez, Grid Converters for Photovoltaic and Wind Power Systems, John Wiley & Sons, 2011, ISBN: 978-1-119-95720-1.

[3] P. Kundur, Power System Stability and Control., McGraw-Hill Education, 1994, ISBN: 978-0-07-035958-1.

[4] Australian Energy Market Operator (AEMO), Power system requirements (jul 2020).

[5] V. Trovato, A. Mazza, G. Chicco, Flexible operation of low-inertia power systems connected via high voltage direct current interconnectors, Electric Power Systems Research (2020) 106911.

[6] Australian Energy Market Operator (AEMO), Analysis of the South Australian Blackout - 28 September 2016, Tech. rep. (2017).

[7] Terna - Rete Elettrica Nazionale S.p.A., Codice di Rete (2020).

[8] ENTSO-E, High Penetration of Power Electronic Interfaced Power Sources and the Potential Contribution of Grid Forming Converters, Technical Report (Jan. 2020).

[9] Terna, Pilot Project Fast Reserve (Jul. 2020).

[10] Fingrid, Fast Frequency Reserve (Jun. 2021).

[11] J. Liu, Y. Miura, T. Ise, Comparison of dynamic characteristics between virtual synchronous generator and droop control in inverter-based distributed generators, IEEE Transactions on Power Electronics 31 (5) (2016) 3600–3611.

[12] R. Bojoi, G. Griva, V. Bostan, M. Guerriero, F. Farina, F. Profumo, Current control strategy for power conditioners using sinusoidal signal integrators in synchronous reference frame, IEEE Transactions on Power Electronics 20 (6) (2005) 1402–1412.

[13] U. Tamrakar, D. Shrestha, M. Maharjan, B. P. Bhattarai, T. M. Hansen, R. Tonkoski, Virtual Inertia: Current Trends and Future Directions, Applied Sciences 7 (7) (2017) 654.

[14] M. Chen, D. Zhou, F. Blaabjerg, Modelling, Implementation, and Assessment of Virtual Synchronous Generator in Power Systems, Journal of Modern Power Systems and Clean Energy 8 (3) (2020) 399–411.

[15] K. R. Vasudevan, V. K. Ramachandaramurthy, T. S. Babu, A. Pouryekta, Synchronverter: A Comprehensive Review of Modifications, Stability Assessment, Applications and Future Perspectives, IEEE Access 8 (2020) 131565–131589.

[16] H. Beck, R. Hesse, Virtual synchronous machine, in: 2007 9th International Conference on Electrical Power Quality and Utilisation, 2007, pp. 1–6.

[17] R. Hesse, D. Turschner, H.-P. Beck, Micro grid stabilization using the virtual synchronous machine, (VISMA), Renewable energy & power quality journal 1 (2009) 676–681.

[18] Y. Chen, R. Hesse, D. Turschner, H.-P. Beck, Dynamic properties of the virtual synchronous machine (VISMA), Renewable energy & power quality journal (2011) 755–759.

[19] Y. P. Chen, R. Hesse, D. Turschner, H.-P. Beck, Comparison of methods for implementing virtual synchronous machine on inverters, Renewable energy & power quality journal (2012) 734–739.

[20] Q. Zhong, G. Weiss, Static synchronous generators for distributed generation and renewable energy, in: 2009 IEEE/PES Power Systems Conference and Exposition, 2009, pp. 1–6.

[21] Q. Zhong, P. Nguyen, Z. Ma, W. Sheng, Self-synchronized synchronverters: Inverters without a dedicated synchronization unit, IEEE Transactions on Power Electronics 29 (2) (2014) 617–630.

[22] S. Rubino, A. Mazza, G. Chicco, M. Pastorelli, Advanced control of inverter-interfaced generation behaving as a virtual synchronous generator, in: 2015 IEEE Eindhoven PowerTech, 2015, pp. 1–6.

[23] M. Blau, G. Weiss, Synchronverters used for damping inter-area oscillations in two-area power systems, Renewable Energy and Power Quality Journal (2018) 45–50.

[24] K. Sakimoto, Y. Miura, T. Ise, Stabilization of a power system with a distributed generator by a virtual synchronous generator function, in: 8th International Conference on Power Electronics - ECCE Asia, 2011, pp. 1498–1505.

[25] Jia Liu, Y. Miura, T. Ise, Dynamic characteristics and stability comparisons between virtual synchronous generator and droop control in inverter-based distributed generators, in: 2014 International Power Electronics Conference (IPEC-Hiroshima 2014 - ECCE ASIA), 2014, pp. 1536–1543.

[26] P. Rodriguez, I. Candela, A. Luna, Control of pv generation systems using the synchronous power controller, in: 2013 IEEE Energy Conversion Congress and Exposition, 2013, pp. 993–998.

[27] W. Zhang, A. Luna, I. Candela, J. Rocabert, P. Rodriguez, An active power synchronizing controller for grid-connected power converters with configurable natural droop characteristics, in: 2015 IEEE 6th International Symposium on Power Electronics for Distributed Generation Systems (PEDG), 2015, pp. 1–7.

[28] P. R. Cortés, J. I. C. Garcia, J. R. Delgado, R. Teodorescu, Virtual controller of electromechanical characteristics for static power cnverters.

[29] P. R. Cortés, J. I. C. Garcia, J. R. Delgado, R. Teodorescu, Synchronous power controller for a generating system based on static power converters.

[30] J. Driesen, K. Visscher, Virtual synchronous generators, in: 2008 IEEE Power and Energy Society General Meeting - Conversion and Delivery of Electrical Energy in the 21st Century, 2008, pp. 1–3.

[31] M. P. N. van Wesenbeeck, S. W. H. de Haan, P. Varela, K. Visscher, Grid tied converter with virtual kinetic storage, in: 2009 IEEE Bucharest PowerTech, 2009, pp. 1–7.

[32] Y. Hirase, K. Abe, K. Sugimoto, Y. Shindo, A grid connected inverter with virtual synchronous generator model of algebraic type, IEEJ Transactions on Power and Energy 132 (2012) 371–380.

[33] Y. Hirase, K. Sugimoto, K. Sakimoto, T. Ise, Analysis of resonance in microgrids and effects of system frequency stabilization using a virtual synchronous generator, IEEE Journal of Emerging and Selected Topics in Power Electronics 4 (4) (2016) 1287–1298.

[34] S. D'Arco, J. A. Suul, O. B. Fosso, Control system tuning and stability analysis of virtual synchronous machines, in: 2013 IEEE Energy Conversion Congress and Exposition, 2013, pp. 2664–2671.

[35] S. D'Arco, J. A. Suul, O. B. Fosso, Small-signal modeling and parametric sensitivity of a virtual synchronous machine in islanded operation, International Journal of Electrical Power & Energy Systems 72 (2015) 3 – 15, the Special Issue for 18th Power Systems Computation Conference.

[36] F. Mandrile, E. Carpaneto, R. Bojoi, Grid-tied inverter with simplified virtual synchronous compensator for grid services and grid support, in: 2019 IEEE Energy Conversion Congress and Exposition (ECCE), 2019, pp. 4317–4323.

[37] F. Mandrile, E. Carpaneto, R. Bojoi, Grid-Feeding Inverter With Simplified Virtual Synchronous Compensator Providing Grid Services and Grid Support, IEEE Transactions on Industry Applications 57 (1) (2021) 559–569.

[38] R. Eriksson, Synthetic inertia versus fast frequency response: a definition, IET Renewable Power Generation 12 (2018) 507–514(7).

[39] C. Diaz-Londono, D. Enescu, F. Ruiz, A. Mazza, Experimental modeling and aggregation strategy for thermoelectric refrigeration units as flexible loads, Applied Energy 272 (2020) 115065.

[40] L. Toma, M. Sanduleac, S. A. Baltac, F. Arrigo, A. Mazza, E. Bompard, A. Musa, A. Monti, On the virtual inertia provision by BESS in low inertia power systems, in: 2018 IEEE International Energy Conference (ENERGYCON), 2018, pp. 1–6.

[41] H. Bevrani, T. Ise, Y. Miura, Virtual synchronous generators: A survey and new perspectives, International Journal of Electrical Power & Energy Systems 54 (2014) 244 – 254.

[42] C. Mosca, F. Arrigo, A. Mazza, E. Bompard, E. Carpaneto, G. Chicco, P. Cuccia, Mitigation of frequency stability issues in low inertia power systems using synchronous compensators and battery energy storage systems, Transmission Distribution IET Generation 13 (17) (2019) 3951–3959.

[43] J. Fang, Y. Tang, H. Li, X. Li, A battery/ultracapacitor hybrid energy storage system for implementing the power management of virtual synchronous generators, IEEE Transactions on Power Electronics 33 (4) (2018) 2820–2824.

[44] W. Wu, Y. Chen, L. Zhou, A. Luo, X. Zhou, Z. He, L. Yang, Z. Xie, J. Liu, M. Zhang, Sequence impedance modeling and stability comparative analysis of voltage-controlled vsgs and current-controlled vsgs, IEEE Transactions on Industrial Electronics 66 (8) (2019) 6460–6472.

[45] F. Mandrile, E. Carpaneto, R. Bojoi, Virtual synchronous generator with simplified single-axis damper winding, in: 2019 IEEE 28th International Symposium on Industrial Electronics (ISIE), 2019, pp. 2123–2128.

[46] X. Wang, P. C. Loh, F. Blaabjerg, Stability analysis and controller synthesis for single-loop voltage-controlled VSIs, IEEE Transactions on Power Electronics 32 (9) (2017) 7394–7404.